Self-catalyzed vapor–liquid–solid growth of InP/InAsP core–shell nanopillars

ARTICLE *in* JOURNAL OF CRYSTAL GROWTH · JANUARY 2011

Impact Factor: 1.7 · DOI: 10.1016/j.jcrysgro.2010.11.092

Journal of Crystal Growth 314 (2011) 34–38

Contents lists available at ScienceDirect

Journal of Crystal Growth

journal homepage: www.elsevier.com/locate/jcrysgro

Self-catalyzed vapor–liquid–solid growth of InP/InAsP core–shell nanopillars

Vanessa Evoen [a], Hailong Zhou [a], Li Gao [a], Marta Pozuelo [b], Baolai Liang [c], Jun Tatebeyashi [c], Suneel Kodambaka [b], Diana L. Huffaker [c], Robert F. Hicks [a,b,*]

[a] Department of Chemical Engineering, University of California Los Angeles, Los Angeles, CA 90095, USA
[b] Department of Materials Science and Engineering, University of California Los Angeles, Los Angeles, CA 90095, USA
[c] Department of Electrical Engineering, University of California Los Angeles, Los Angeles, CA 90095, USA

ARTICLE INFO

Article history:
Received 18 September 2010
Received in revised form
30 October 2010
Accepted 11 November 2010
Communicated by J.M. Redwing
Available online 19 November 2010

Keywords:
A1. Nanopillars
A3. Metalorganic vapor phase epitaxy
B2. InP/InAsP

ABSTRACT

Indium phosphide/indium arsenide phosphide core–shell nanopillars have been prepared by the vapor–liquid–solid method using liquid indium droplets as the catalyst. The indium droplets were generated in situ in the deposition reactor. The hexagonal nanopillars exhibited hexagonal shaped sidewalls with average width and height of 150 and 250 nm, respectively. Cross-section transmission electron microscopy with selected area electron diffraction and X-ray dispersion energy analysis verified that an InAsP layer, approximately 10 nm thick, coated the pillars. Photoluminescence spectra at 77 K yielded an extremely intense band at 0.76 eV (1.63 μm), which was due to the InAsP shell on the pillars.

1. Introduction

Compound semiconductor nanowires are promising materials for nanoscale electronic and photonic devices [1–4]. Heterojunctions have been fabricated by growing core–shell nanowires with the carriers confined along the wire axis to one dimension [5–7]. Core–shell structures suppress surface states on the sidewalls, thereby reducing scattering and yielding high carrier mobility [6,8]. Potential applications of nanowires include light-emitting diodes, laser diodes, single photon and electron sources, photodetectors, heterojunction transistors, sensors, solar cells, and battery anodes [2,8–14].

It is well known that nanowires may be grown by the metal-catalyzed vapor–liquid–solid (VLS) process [15], in which reactant species from the vapor phase are absorbed by the liquid droplets, which deposit the III/V crystal at the liquid–solid interface. A broad range of compound semiconductor core–shell structures have been synthesized by different growth methods, including metalorganic vapor phase epitaxy (MOVPE), molecular beam epitaxy (MBE), pulse laser deposition (PLD), and chemical beam epitaxy (CBE) [16–24]. The III–V ternary alloy InAsP is an interesting material because its direct energy band gap covers the range from 1.35 to 0.35 eV (InP to InAs), which covers the technologically important wavelength ranging around 1.3 and 1.55 μm [25,26]. In most cases, gold droplets have been used to catalyze the VLS process [21,23–26]. Relatively few publications have considered self-catalysis of III/V nanowires using group III liquid droplets. In our group, we have shown that InP nanowires, nanocones, and nanopillars can be grown using indium droplets on InP(1 1 1)B by precisely controlling the growth temperature and V/III ratio [27].

In this paper, we demonstrate that the InP/InAsP core–shell nanopillars can be prepared by self-catalyzed VLS of InP pillars, followed by the deposition of an InAsP shell and InP cap layer. These nanostructures are single crystal wurtzite but with a relatively high density of twins and stacking faults along the growth direction. Photoluminescence spectra of the core–shell structure and of a reference sample without the nanopillars demonstrate that the InAsP shells on the nanopillars produce intense emission at 0.76 eV (1.63 μm).

2. Experimental methods

The experiments were carried out in a Veeco D125 MOVPE reactor using trimethylindium (TMIn), tertiarybutylphosphine (TBP), and tertiarybutylarsine (TBA) as precursors. The nanostructures were grown on the InP(1 1 1)B substrates. The substrate temperature was ramped to between 390 and 400 °C, and indium droplets were deposited by feeding 5.06×10^{-5} mol/min of TMIn for 12 s. Then TMIn and TBP were introduced into the reactor at flow rates of 3.74×10^{-6} and 3.37×10^{-4} mol/min (V/III ratio=90), respectively, to grow the InP nanopillars. After 9 min,

* Corresponding author at: Department of Chemical Engineering, University of California Los Angeles, Los Angeles, CA 90095, USA. Tel.: +1 310 206 6865; fax: +1 310 206 4107.
E-mail addresses: hailong@ucla.edu (H. Zhou), rhicks@ucla.edu (R.F. Hicks).

0022-0248/$ - see front matter © 2010 Elsevier B.V. All rights reserved.
doi:10.1016/j.jcrysgro.2010.11.092

the reactor was purged with H_2 for 10 s and then with TBA for 3 min while the temperature was ramped up to 420 °C. Following the interrupt, the InAs shell was deposited on the InP nanopillars by flowing TBA at 9.82×10^{-3} mol/min with a TMIn flow of 8.18×10^{-5} mol/min (V/III ratio=120). The InAs growth time was 10 s. The reactor was purged with H_2 for 10 s and with TBP for 1 min, and an InP cap layer was deposited by feeding 3.73×10^{-6} mol/min of TMIn and 3.37×10^{-3} mol/min of TBP (V/III ratio=90) for 1 min. Finally, the sample was cooled down and removed from the reactor for characterization. The total pressure in the reactor was maintained at 60 Torr. A reference sample was prepared by the same procedure given above, except that the indium droplet deposition step was omitted.

The morphology of the pillars was studied using a FEI Nova 600 Nanolab DualBeam focused-ion-beam (FIB) scanning electron microscope at an acceleration voltage of 10 kV. The data were processed with the aid of Image J. Multiple scanning electron microscopy (SEM) images were analyzed to obtain the average diameter, width, and height. High resolution transmission electron microscopy (HRTEM) images and selected area electron diffraction (SAED) patterns were obtained using a FEI Titan 300 kV scanning transmission electron microscope equipped with an energy dispersive X-ray (EDX) detector. For this purpose, the nanopillars were exfoliated from the substrate and placed on a TEM grid for the normal HRTEM. A cross-sectional TEM sample of the core–shell pillars was prepared by the focus-ion-beam (FIB). Initially, we deposited Pt in order to cover all the free areas around the pillars. The deposition was first made by the electron-beam to prevent any damage on the sample and second by the ion-beam. After that, ion-beam milling at the site of interest gave a very thin film transparent enough for TEM characterization. Photoluminescence (PL) measurements were made on the core–shell and reference samples at 77 K using the 659 nm line of a diode laser with laser spot size about 100 μm in diameter.

3. Results and discussion

Shown in Fig. 1 is a side-view SEM image of the InP/InAsP core–shell nanopillars. These structures have a hexagonal shape with slight tapering, and the average width and height are 150 and 250 nm, respectively. In addition, they have hexagonal skirts that are ~275 nm wide. The pillars are short and fat due to the relatively high growth temperature. This shape can be explained by the competition between two growth mechanisms: vapor–liquid–solid (VLS), which occurs primarily in the vertical direction; and vapor phase epitaxy (VPE), which occurs mainly in the lateral direction [27]. According to our previous study, the VPE rate increases relative to the VLS rate as one raises the substrate temperature. At 400 °C, VPE is significant so that lateral and vertical growth occurs simultaneously, giving rise to nanopillars.

A TEM image of a single InP/InAsP core–shell nanopillar is presented in Fig. 2(a). Twins and stacking faults aligned perpendicular to the [0 0 0 1] growth direction are clearly visible in the picture. In the higher-resolution TEM image (Fig. 2(b)), a twin is highlighted by the bracket while two stacking faults are indicated by the arrows. The SAED pattern in Fig. 2(c) reveals a wurtzite (WZ) crystal structure along the [2 $\bar{1}$ $\bar{1}$ 0] zone axis. Note that the streaks in the [0 0 0 1] direction are indicative of the defects oriented perpendicular to this axis.

A TEM image of a thin slice through an InP/InAsP core–shell nanopillar is shown in Fig. 3(a). One can discern a graded region around the perimeter of the pillar that is due to the InAsP shell. Separate InAs shell and InP cap layers are not evident, and suggest that the arsenic and phosphorus atoms inter-diffuse to yield a graded $InAs_xP_{1-x}$ alloy. Fukui's group could grow 10 nm InAs shell on InP core at relatively similar condition (400 °C with V/III ratio of 128) using selective area MOVPE [28]; however they did not make any detail observation on the InAs/InP interfaces. Here, we show the possible graded As composition that could occur on the interfaces between the InP core and InAs shell. The SAED pattern in Fig. 3(b) is indicative of the wurtzite crystal structure oriented parallel to the [0 0 0 1] zone axis. The set of {1 $\bar{1}$ 0 0} planes are the side facets to the nanopillars. The arrows in the electron diffraction pattern highlight two diffraction spots corresponding to InP and $InAs_xP_{1-x}$. The spots closer to the direct beam correspond to the latter material. Note that the relative intensities of the pairs vary widely among the reflections and is most likely the result of a slight degree of tilt from the zone axis. The interplanar distances measured for each of the InP diffraction spots agree to within 0.3% and correspond to a lattice parameter of 0.415 nm. The measured lattice parameter for the alloy was 0.424 nm. With this value and applying Vegard's law, it was estimated that the $InAs_xP_{1-x}$ composition was $x=0.7 \pm 0.1$.

An EDX line-scan was performed along the cross-section of the pillar. The elemental counts as a function of the position are presented in Fig. 3(c). The blue, red, and green lines correspond to arsenic, indium, and phosphorus, respectively. An arsenic-rich

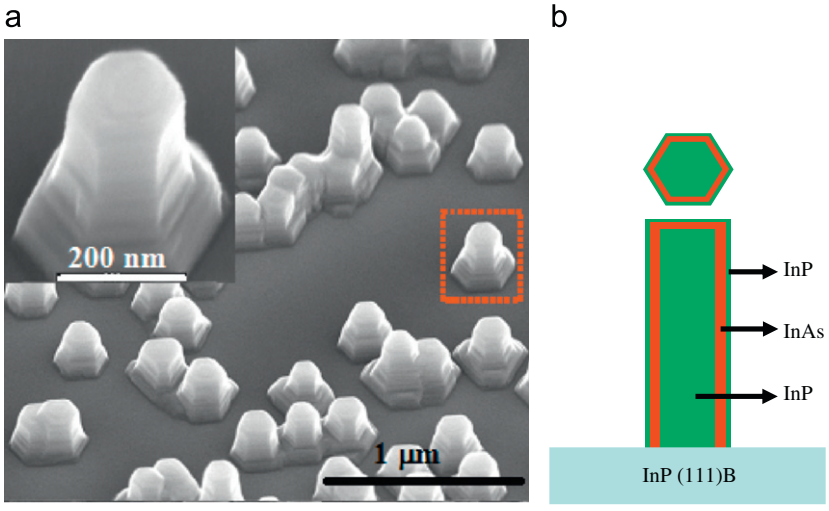

Fig. 1. Scanning electron micrograph of (a) InP/InAsP core–shell nanopillars (viewing angle=52°); the inset image is of the pillar highlighted by the red square and (b) schematic diagram of the core–shell nanopillars. (For interpretation of the references to colour in this figure legend, the reader is referred to the web version of this article.)

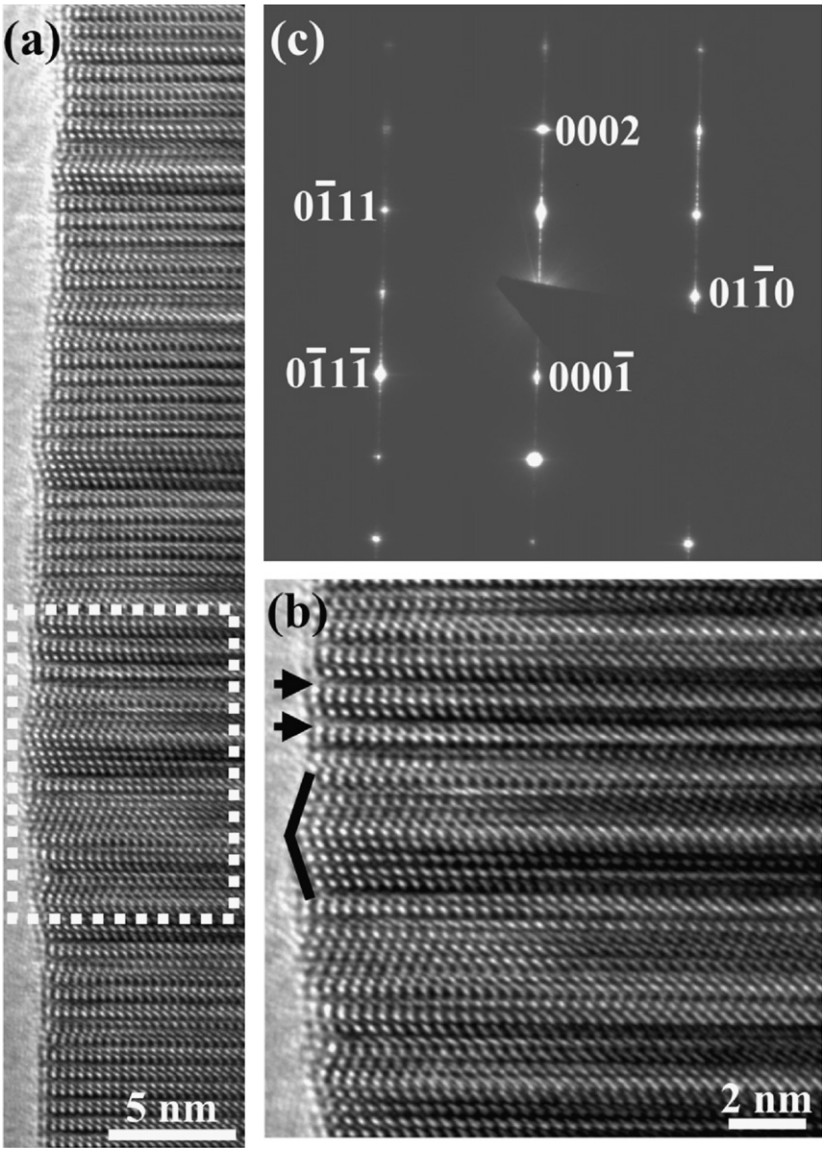

Fig. 2. Transmission electron micrograph and selected area electron diffraction pattern of an individual pillar: (a) bright-field image; (b) higher magnification image of the region highlighted in (a) where a twin and two stacking faults are indicated by a bracket and arrows, respectively; and (c) SAED of the pillar indexed as wurtzite along the[2 $\bar{1}$ $\bar{1}$ 0] zone axis.

region is observed at the edge of the pillar, confirming the presence of a graded InAsP shell around the InP core. Although InP cap layer growth was added at the end of the growth sequence, this does not appear to be successful, either due to As and P inter-diffusion, or to As segregation at the growth front under the conditions present in the MOCVD reactor.

The optical properties of the InP/InAsP core–shell nanopillars were characterized by photoluminescence at 77 K. A reference sample was grown with the same recipe as that of the core–shell nanopillars, except that the indium droplet deposition step was left out. The emission spectra from the core–shell nanopillars and the reference sample are presented in Fig. 4. The micrographs in the upper right-hand corner of the graph show the surface structure over which each spectrum was acquired. The reference sample exhibits two sharp peaks at 1.38 and 0.69 eV due to bulk zinc-blende indium phosphide. In addition, there are two broad bands at 1.14 and 0.99 eV that arise from the 3-dimensional InP/InAsP film on the InP(1 1 1)B substrate. The PL spectrum of the nanopillars contains the same four features seen in the reference sample, and in addition, exhibits an intense band at 0.76 eV. The signal-to-noise ratio of this peak exceeds 100. This emission is attributed to the InAsP shell on the nanopillars.

In Fig. 5, the PL spectrum of the core–shell nanopillars has been deconvoluted by fitting it to 3 Gaussian peaks. The peak with a maximum at 0.76 eV has a full-width-at-half-maximum (FWHM) of 100 meV. Assuming the $InAs_xP_{1-x}$ layer to be that of a homogeneous bulk alloy, a 0.76 eV band gap energy would correspond to an arsenic content of $x=0.65$. This value is consistent with that estimated from the splitting of the SAED spots. Nevertheless, the PL spectrum was obtained from about 1000 nanopillars, which exhibited a broad distribution of widths ranging from 100 to 180 nm. With changing width (i.e., growth rate) of the nanopillars, the thickness and the composition of the InAsP shell could vary significantly, and would explain why an FWHM of 100 meV is observed. For example, in AlGaAs nanowire growth, a PL emission peak was recorded for the alloy with a similar broad width, and this has been attributed to variations in the alloy composition [31,32].

Samuelson's group [29] has grown InAs cores (~20–45 nm thick) and InP shells (~20 nm thick) by VLS using gold catalysis. They observed a photoluminescence peak at 0.7–0.8 eV, which was

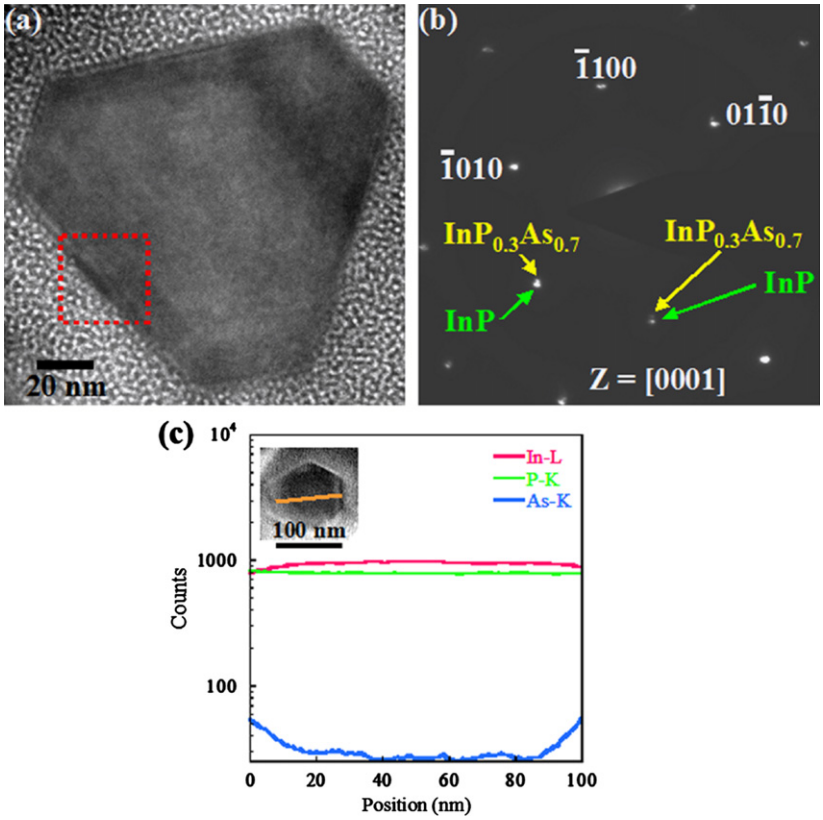

Fig. 3. (a) Cross-section TEM image of a single InP/InAsP core–shell nanopillar, (b) selected area electron diffraction of the area highlighted in (a), and (c) EDS data of As–K (blue curve) and P–K (green curve) line intensities, normalized with respect to In–L (red curve) line intensity, plotted as a function of position along the line on the pillar shown in the STEM image as inset. (For interpretation of the references to colour in this figure legend, the reader is referred to the web version of this article.)

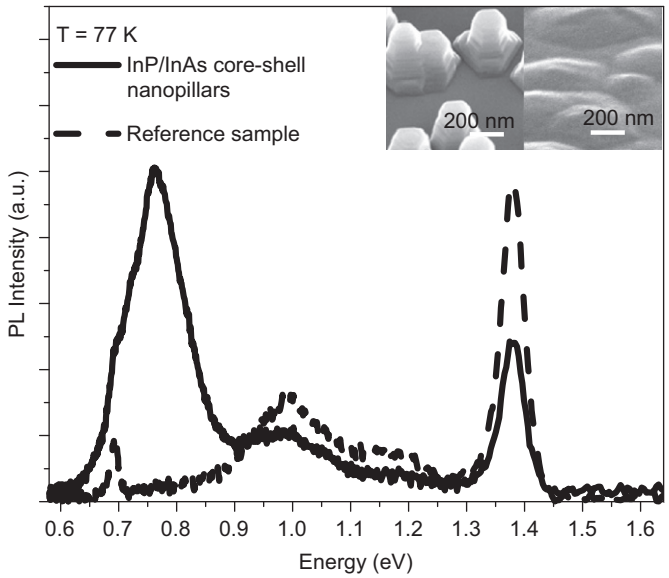

Fig. 4. Photoluminescence spectra at 77 K of InP/InAsP core–shell nanopillars and the reference sample. The SEM images (viewed at 45°) in the upper right corner of the graph are of the core–shell nanopillars and the reference sample.

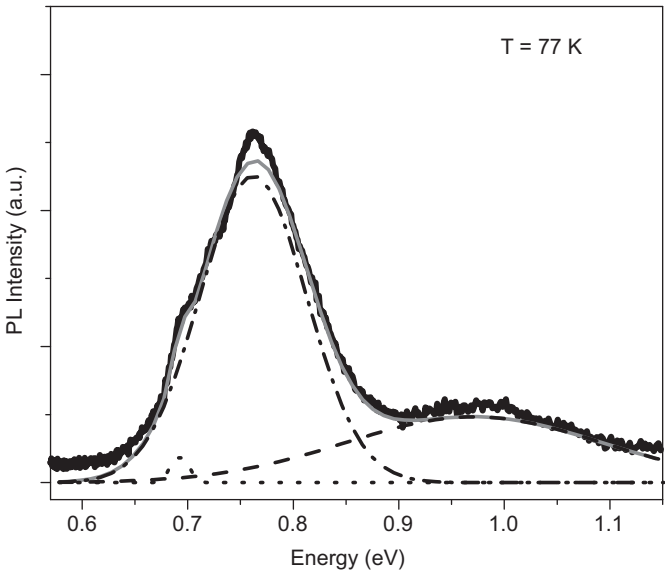

Fig. 5. Deconvolution of the nanopillar photoluminescence spectrum using three Gaussian peaks.

due to the InAs core nanowire, although the signal-to-noise ratio of their emission was atleast an order of magnitude less than that obtained in the present study. Harmand's group [25] prepared InP/InAsP axial heterostructures in nanowires and obtained two extremely narrow peaks at about 0.88 eV by micro-PL on single wires. Furthermore, InAsP/InP quantum-well heterostructures grown on InP (0 0 1) exhibit emission lines below 0.8 eV when the thickness of the $InAs_{0.65}P_{0.35}$ well exceeds 10 nm [30]. A comparison of this work to the data presented here fully supports our conclusion that an InAsP heterojunction shell was deposited on the InP nanopillars by the self-catalyzed VLS technique.

A close examination of the photoluminescence spectrum does not reveal the presence of wurtzite indium phosphide, which emits higher energy at 84 meV than that for zinc-blende indium

phosphide. There are several possible explanations for this. The intensity of the emission from the WZ nanopillars may be only a small fraction of that produced from the ZB substrate, so that it cannot be seen beneath the latter emission. Alternatively, the wurtzite emission may be suppressed by recombination from type II band alignment, which could occur as a result of the stacking faults and twins in the nanopillars, cf., Fig. 2 [33,34].

4. Conclusions

We have demonstrated the growth of single-crystal InP/InAsP core–shell nanopillars on InP(1 1 1)B. These structures were prepared by self-catalyzed VLS using liquid indium droplets that were generated in situ in the MOVPE reactor. Cross-section TEM combined with SAED and EDX, together with photoluminescence at 77 K of the core–shell and reference samples, indicated that a graded InAsP alloy layer about 10 nm thick was deposited over the InP nanopillars. The $InAs_xP_{1-x}$ shell exhibited intense broad emission at 0.76 eV, which is in good agreement with the alloy composition estimated from SAED of $x=0.7\pm0.1$. These results suggest that self-catalyzed VLS may be a viable method of generating heterojunctions on nanopillars in the wavelength range of 1.3–1.5μm.

Acknowledgments

This work was supported by funds from Intel Corporation, Northrop Grumman Space Technologies and UC Discovery. Dr. Kodambaka gratefully acknowledges support from the NSF though the Grant CMMI-0926412.

References

[1] W. Lu, P. Xie, C.M. Lieber, IEEE Trans. Electron Devices 55 (2008) 2859.
[2] X. Duan, Y. Huang, R. Agarwal, C.M. Lieber, Nature 421 (2003) 241.
[3] M.T. Björk, C. Thelander, A.E. Hansen, L.E. Jensen, M.W. Larsson, L.R. Wallenberg, L. Samuelson, Nano Lett. 4 (2004) 1621.
[4] W.U. Huynh, J.J. Dittmer, A.P. Alivisatos, Science 295 (2002) 2425.
[5] L.J. Lauhon, M.S. Gudiksen, D. Wang, C.M. Lieber, Nature 420 (2002) 57.
[6] X. Jiang, Q. Xiong, S. Nam, F. Qian, Y. Li, C.M. Lieber, Nano Lett. 7 (2007) 3214.
[7] L.F. Cui, Y. Yang, C.M. Hsu, Y. Cui, Nano Lett. 9 (2009) 3370.
[8] Q. Kuang, C. Lao, Z.L. Wang, Z. Xie, L. Zheng, J. Am. Chem. Soc. 129 (2007) 6070.
[9] Y. Cui, Q. Wei, H. Park, C.M. Lieber, Science 293 (2001) 1289.
[10] Y. Cui, C.M. Lieber, Science 291 (2001) 851.
[11] A. Fuhrer, C. Fasth, L. Samuelson, Appl. Phys. Lett. 91 (2007) 052109.
[12] E.D. Minot, F. Kelkensberg, M. van Kouwen, J.A. van Dam, L.P. Kouwenhoven, V. Zwiller, M.T. Borgström, O. Wunnicke, M.A. Verheijen, E.P.A.M. Bakkers, Nano Lett. 7 (2007) 367.
[13] B. Tian, X. Zheng, T.J. Kempa, Y. Fang, N. Yu, G. Yu, J. Huang, C.M. Lieber, Nature 449 (2007) 885.
[14] Z.L. Wang, J.H. Song, Science 312 (2006) 242.
[15] S. Wagner, W.C. Ellis, Appl. Phys. Lett. 4 (1964) 89.
[16] A.I. Hochbaum, R. Fan, R. He, P. Yang, Nano Lett. 5 (2005) 457.
[17] S.D. Hersee, X. Sun, X. Wang, Nano Lett. 6 (2006) 1808.
[18] T. Kuykendall, P.J. Pauzauskie, Y. Zhang, J. Goldberger, D. Sirbuly, J. Denlinger, P. Yang, Nat. Mater. 3 (2004) 524.
[19] K.K. Lew, L. Pan, E.C. Dickey, J.M. Redwing, Adv. Mater. 15 (2003) 2073.
[20] W. Liang, O. Rabin, A. Hochbaum, M. Fardy, M. Zhang, P. Yang, Nano Res. 2 (2009) 394.
[21] H. Peng, D.T. Schoen, S. Meister, X.F. Zhang, Y. Cui, J. Am. Chem. Soc. 129 (2007) 34.
[22] L. Greene, M. Law, B. Yuhas, P. Yang, J. Phys. Chem. C 111 (2007) 18451.
[23] S. Xu, N. Adiga, S. Ba, T. Dasgupta, C.F. Jeff Wu, Z.L. Wang, ACS Nano 3 (2009) 1803.
[24] Q. Kuang, C.S. Lao, Z. Li, Z.X. Xie, L.S. Zheng, Z.L. Wang, J. Phys. Chem. C 112 (2008) 11539.
[25] M. Tchernycheva, G.E. Cirlin, G. Patriarche, L. Travers, V. Zwiller, U. Perinetti, J.-C. Harmand, Nano Lett. 7 (2007) 1500.
[26] H. Pettersson, J. Tragardh, A.I. Persson, L. Landin, D. Hessman, L. Samuelson, Nano Lett. 6 (2006) 229.
[27] R. Woo, L. Gao, N. Goel, M. Hudait, K.L. Wang, S. Kodambaka, R.F. Hicks, Nano Lett. 9 (2009) 2207.
[28] P. Mohan, J. Motohisa, T.i Fukui, Appl. Phys. Lett. 88 (2006) 013110.
[29] Z. Zanolli, M.–E. Pistol, L.E. Fröberg, L. Samuelson, J. Phys. Condens. Matter 19 (2007) 295219.
[30] A. Kasukawa, T. Namegaya, T. Fukushima, N. Iwai, T. Kikuta, J. IEEE, Quantum Electron. 29 (1993) 1528.
[31] H.L. Zhou, T.B. Hoang, D.L. Dheeraj, A.T.J. van Helvoort, L. Liu, J.-C. Harmand, B.O. Fimland, H. Weman, Nanotechnology 20 (2009) 415701.
[32] C. Chen, S. Shehata, C. Fradin, R.R. LaPierre, C. Couteau, G. Weihs, Nano Lett. 7 (2007) 2584.
[33] J.M. Bao, D.C. Bell, F. Capasso, J.B. Wagner, T. Mårtensson, J. Trägårdh, L. Samuelson, Nano Lett. 8 (2008) 836.
[34] P. Caroff, K. Dick, J. Johansson, M. Messing, K. Deppert, L. Samuelson, Nat. Nanotechnol. 4 (2009) 50.